Energies **2015**, *8*, 1373-1389; doi:10.3390/en8021373

OPEN ACCESS

energies

ISSN 1996-1073

www.mdpi.com/journal/energies

Article

A Reflex Charger with ZVS and Non-Dissipative Cells for Photovoltaic Energy Conversion

Cheng-Tao Tsai *, Ying-Che Kuo, Ying-Piao Kuo and Chin-Tsung Hsieh

Department of Electrical Engineering, National Chin-Yi University of Technology, Taichung 41170, Taiwan; E-Mails: kuoyc@ncut.edu.tw (Y.-C.K.); kuoyp@ncut.edu.tw (Y.-P.K.); fred@ncut.edu.tw (C.-T.H.)

* Author to whom correspondence should be addressed; E-Mail: cttsai@ncut.edu.tw; Tel.: +886-4-2392-4505 (ext. 7240); Fax: +886-4-2392-4419.

Academic Editor: Enrico Sciubba

Received: 30 October 2014 / Accepted: 22 January 2015 / Published: 11 February 2015

Abstract: In this paper, a reflex charger with zero-voltage-switching (ZVS) and non-dissipative cells for photovoltaic (PV) energy conversion is presented. The proposed reflex charger has the following advantages: (1) A ZVS cell is incorporated to reduce the switching losses of the main and auxiliary switches. Therefore, the conversion efficiency of the proposed reflex charger can be improved significantly; (2) A non-dissipative charging/discharging reflex cell is used to increase charging efficiency and extend lifecycle of battery. Finally, a prototype reflex charger with ZVS and non-dissipative cells is built and implemented. Experimental results are presented to verify the performance and the feasibility of the proposed reflex charger for PV energy conversion.

Keywords: zero-voltage-switching; non-dissipative; photovoltaic

1. Introduction

Due to the rapid growth of global energy demand for developing industry, the overuse of fossil fuels results in environmental pollution, greenhouse effects and ecological damage. Adopting renewable and clean energy resources to replace fossil fuels is imperative. To reduce greenhouse effects, the demand for renewable energies has increased significantly. Among renewable energies, PV energy attracts more interest owing to its noiseless, pollution-free, non-radioactive, and inexhaustible characteristics [1,2].

Currently, PV energy is converted into electric power through PV panels. The output voltage and current of PV panels vary nonlinearly with irradiation, panel temperatures and loading conditions. Due to their unstable and intermittent characteristics, PV panels cannot provide a constant or stable power output. Thus, to achieve PV energy conversion, PV panels often adopt chargers and batteries [3–10].

PV panels usually need battery charger charging strategies such as the constant current (CC), constant voltage (CV), hybrid CC/CV and reflex charging strategies to increase the utility rate of energy storage. The CC, CV and hybrid CC/CV are simple charging methods. Figure 1 shows the charge methods of these strategies. However, their disadvantages are overcharging and temperature rise, resulting in the degradation of battery life.

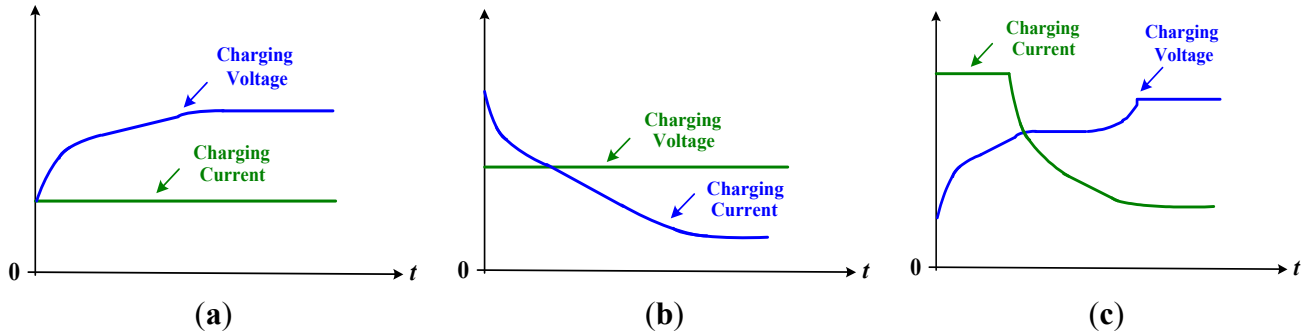

Figure 1. Simple charging strategies: (**a**) charging curve of CC; (**b**) charging curve of CV; and (**c**) charging curve of hybrid CC/CV.

In order to reduce charging time and extend lifecycle of battery, the charging/discharging reflex method is often adopted [11–14]. The charging/discharging waveform of the reflex charger is shown in Figure 2. The method consists of a charging period, a discharging period and a rest period. The charging period function the can reduce battery's charging time, the discharging period function can reduce battery's internal temperature and concentration polarization, and the rest period function can provide the battery's rest time. Therefore, the increased charging efficiency and extended lifecycle of battery are clear [15–22].

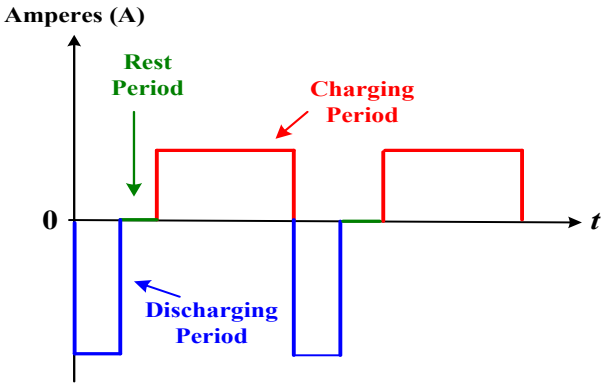

Figure 2. Charging/discharging reflex cycle.

A number of single-stage chargers have been developed and proposed. For example, Buck, Cuk, Zeta and SEPIC converters are adopted, which have simple constructions. However, the active switches of these converters are operated under hard-switching conditions resulting in one of the following

disadvantages: (1) high switching losses; (2) high electromagnetic interference (EMI); and (3) low conversion efficiency. To address these disadvantages, a soft-switching technique called ZVS is used [23,24].

In this paper, a reflex charger with ZVS and non-dissipative cells for PV energy conversion is presented, as shown in Figure 3. The proposed reflex charger incorporates a ZVS cell to reduce the switching losses of the active switches and incorporates a non-dissipative charging/discharging reflex cell to extend lifecycle of battery. To obtain a fast dynamic response algorithm and a protected scheme, a microcontroller is added and presented to implement the optimum control of the proposed reflex charger. The operational principles of the proposed reflex charger are described in Section 2. The control scheme of the proposed reflex charger is described in Section 3. Experimental results obtained from a prototype with the proposed reflex charger for PV energy conversion are presented in Section 4. Finally, a conclusion is given in Section 5.

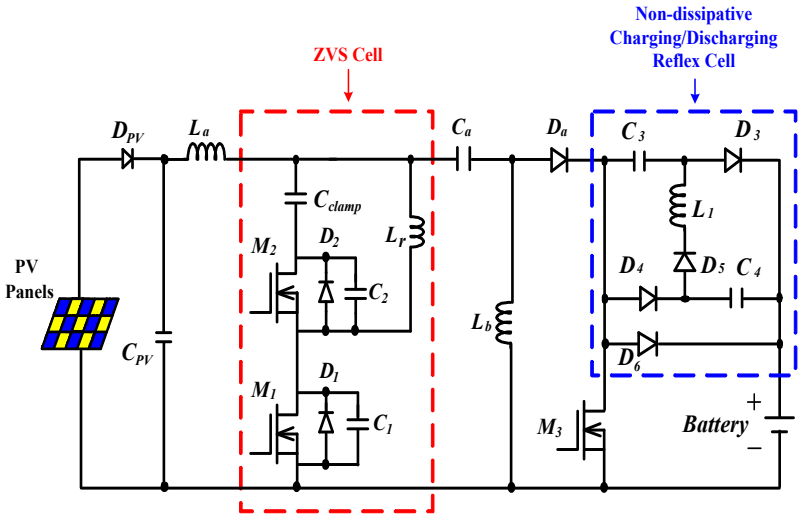

Figure 3. Circuit structure of the proposed reflex charger with ZVS and non-dissipative cells for PV energy conversion.

2. Operational Principles

In Figure 3, the proposed reflex charger includes a ZVS and a non-dissipative charging/discharging reflex cell. The ZVS cell consists of a main switch (M_1), an auxiliary switch (M_2), a resonant inductor (L_r) and a clamp capacitor (C_{clamp}). The non-dissipative charging/discharging reflex cell uses only passive elements (diodes, capacitors and inductors) to implement charging efficiency and extended lifecycle of battery. For convenience of illustration and analysis, the PV panels of Figure 3 can be seen as a constant voltage source. This is simplified and redrawn in Figure 4.

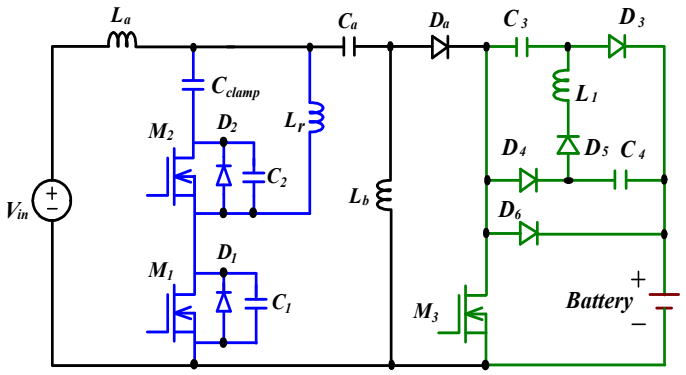

Figure 4. Simplified circuit diagram of the proposed reflex charger.

Figure 5 shows conceptual current and voltage waveforms of the key components and the driving signal switches (M_1, M_2 and M_3) to facilitate the operational principle.

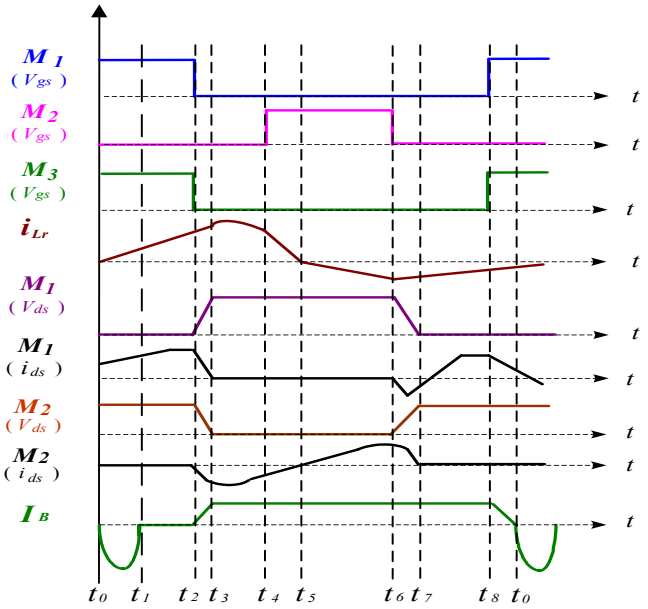

Figure 5. Driving signals of active switches and conceptual current and voltage waveforms of key components.

Figure 6 shows the topological modes of the proposed reflex charger during a switching cycle. To simplify the description of the operational modes, the following assumptions are made:

(1) To analyze the ZVS feature, the body diodes (D_1 and D_2) and parasitic capacitors (C_1 and C_2) of the active switches (M_1 and M_2) will be considered at the steady-state operation of the circuit.

(2) All of components are ideal.

The proposed charger for the reflex charging/discharging mode can be divided into eight modes and explained mode by mode as follows:

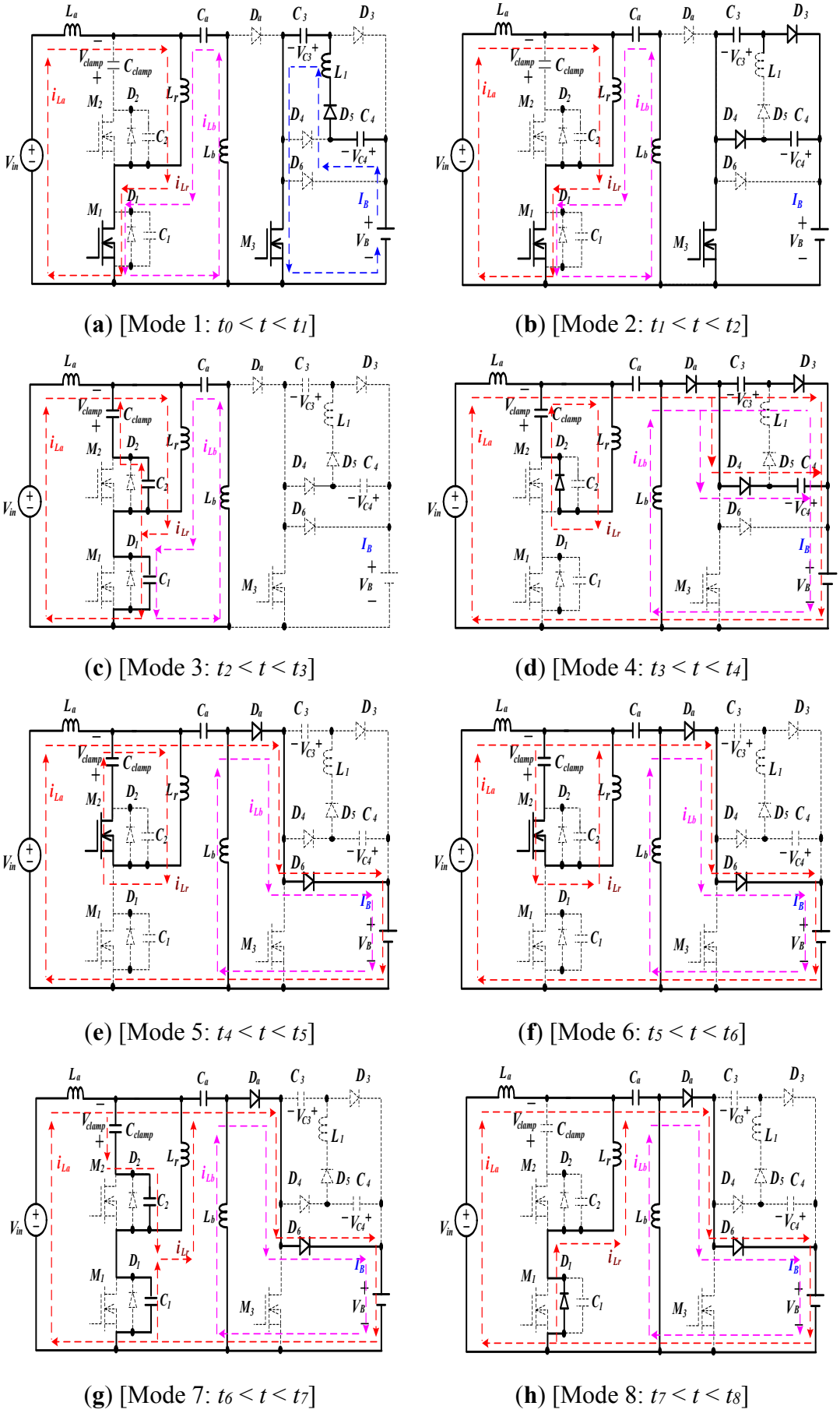

(**a**) [Mode 1: $t_0 < t < t_1$] (**b**) [Mode 2: $t_1 < t < t_2$]

(**c**) [Mode 3: $t_2 < t < t_3$] (**d**) [Mode 4: $t_3 < t < t_4$]

(**e**) [Mode 5: $t_4 < t < t_5$] (**f**) [Mode 6: $t_5 < t < t_6$]

(**g**) [Mode 7: $t_6 < t < t_7$] (**h**) [Mode 8: $t_7 < t < t_8$]

Figure 6. Equivalent circuits of operating modes for the proposed reflex charger.

Mode 1 [Figure 6a, $t_0 < t < t_1$]:

At time t_0, the driving signals of the active switches M_1 and M_3 are turned on, and the current i_{La} and i_{Lb} are flowing through resonant inductor L_r and the active switch M_1. Simultaneously, the battery is discharged through the components (C_4, D_5, L_1, C_3 and M_3) of the non-dissipative charging/discharging reflex cell, as shown in Figure 6a. During this interval, the current of resonant inductor i_{Lr} and discharging current I_B of the battery can be expressed as:

$$i_{Lr}(t) = i_{La}(t - t_0) + i_{Lb}(t - t_0) \tag{1}$$

$$I_{\mathrm{B}} = V_B \sqrt{\frac{C}{2L_1}} \sin[\omega_0 (t - t_0)] \tag{2}$$

where $C = C_3 = C_4$, and $\omega_0 = \sqrt{\frac{2}{L_1 C}}$. The voltage on the capacitor (C_3 and C_4) can be expressed as:

$$V_{C3} = V_{C4} = V_B[1 - \cos\omega_0 (t - t_0)] \tag{3}$$

Mode 2 [Figure 6b, $t_1 < t < t_2$]:

When the charging voltage of capacitors (C_3 and C_4) is equal to the battery voltage (V_B), the battery will stop its discharging action and stay in a rest interval. During this interval, the current of resonant inductor i_{Lr} and discharging current I_B of the battery can be expressed as:

$$i_{Lr}(t) = i_{La}(t - t_1) + i_{Lb}(t - t_1) \tag{4}$$

$$I_{\mathrm{B}} = 0 \tag{5}$$

The voltage on the capacitor (C_3 and C_4) can be expressed as:

$$V_{C3} = V_{C4} = V_B \tag{6}$$

The equivalent circuit is shown in Figure 6b.

Mode 3 [Figure 6c, $t_2 < t < t_3$]:

The driving signals of the switches M_1 and M_3 are turned off at time t_2, and resonant inductor L_r resonates with the parasitic capacitor C_1 of the switch M_1 and the parasitic capacitor C_2 of the switch M_2. Due to the charging time of the parasitic capacitor C_1 of the switch M_1 is very short, the voltage of the switch M_1 will raise steeply. During this interval, the current of the resonant inductor i_{Lr} and discharging current I_B of the battery can be expressed as:

$$i_{Lr}(t) = i_L(t_2) + \frac{V_{in}}{L_a + L_b + L_r}(t - t_2) \tag{7}$$

$$I_{\mathrm{B}} = 0 \tag{8}$$

The equivalent circuit is shown in Figure 6c.

Mode 4 [Figure 6d, $t_3 < t < t_4$]:

At time t_3, the parasitic capacitor C_1 of the switch M_1 is charged to V_{clamp} and the parasitic capacitor C_2 of the switch M_2 is discharged down to zero. The switch M_1 is completely turned off and capacitors C_3 and C_4 of non-dissipative reflex cell will be discharged. Simultaneously, the inductor current i_{Lr} forces the body diode D_2 of M_2 to be conducting and diverts to clamping capacitor C_{clamp} continuously. When the body diode D_2 of the switch M_2 is conducted, a ZVS feature will be created for the switch M_2. During this interval, the current of resonant inductor i_{Lr}, the clamping voltage of clamping capacitor C_{clamp} and charging current of battery can be expressed as:

$$i_{Lr}(t) = i_{Lr}(t_3)\cos\omega(t-t_3) - V_{clamp}(t_3)\sqrt{\frac{C_{clamp}}{L_r}}\sin\omega(t-t_3) \tag{9}$$

$$V_{clamp}(t) = i_{Lr}(t_3)\sin\omega(t-t_3) + V_{clamp}(t_3)\sqrt{\frac{L_r}{C_{clamp}}}\cos\omega(t-t_3) \tag{10}$$

$$I_B = i_{La}(t_3) + i_{Lb}(t_3) \tag{11}$$

where $\omega = \sqrt{\frac{1}{L_r C_{clamp}}}$. The equivalent circuit of mode 4 is shown in Figure 6d.

Mode 5 [Figure 6e, $t_4 < t < t_5$]:

At time t_4, the switch M_2 is turned on under ZVS conditions. During this interval, the capacitors C_3 as well as C_4 are discharged to zero, and diode D_6 is conducted. The currents i_{La} and i_{Lb} begin flowing through the diode D_6, and charge to the battery. During this interval, the current of resonant inductor i_{Lr}, the clamping voltage of clamping capacitor C_{clamp} and charging current of battery can be expressed as:

$$i_{Lr}(t) = i_{Lr}(t_4)\cos\omega(t-t_4) - V_{clamp}(t_4)\sqrt{\frac{C_{clamp}}{L_r}}\sin\omega(t-t_4) \tag{12}$$

$$V_{clamp}(t) = i_{Lr}(t_4)\sin\omega(t-t_4) + V_{clamp}(t_4)\sqrt{\frac{L_r}{C_{clamp}}}\cos\omega(t-t_4) \tag{13}$$

$$I_B = i_{La}(t_4) + i_{Lb}(t_4) \tag{14}$$

The equivalent circuit of mode 5 is shown in Figure 6e.

Mode 6 [Figure 6f, $t_5 < t < t_6$]:

When the resonant inductor current i_{Lr} reaches zero at time t_5, it will be reversed and flow through the resonant inductor L_r. At this interval, the battery is continuously charged. During this interval, the current of resonant inductor i_{Lr}, the clamping voltage of clamping capacitor C_{clamp} and charging current of battery can be expressed as:

$$i_{Lr}(t) = -V_{clamp}(t_5)\sqrt{\frac{C_{clamp}}{L_r}}\sin\omega(t-t_5) \tag{15}$$

$$V_{clamp}(t) = V_{clamp}(t_5)\sqrt{\frac{L_r}{C_{clamp}}}\cos\omega(t-t_5) \tag{16}$$

$$I_B = i_{La}(t_5) + i_{Lb}(t_5) \tag{17}$$

The equivalent circuit of mode 6 is shown in Figure 6f.

Mode 7 [Figure 6g, $t_6 < t < t_7$]:

The switch M_2 is turned off at time t_6, and resonant inductor L_r resonates with the parasitic capacitor C_1 of the switch M_1 and the parasitic capacitor C_2 of the switch M_2. Due to the charging time of the parasitic capacitor C_2 is very short, the voltage of the switch M_2 will be steeply raised. During this interval, the currents i_{La} and i_{Lb} will flow through the diode D_6 and the battery continuously. The current of resonant inductor i_{Lr}, the clamping voltage of clamping capacitor C_{clamp} and charging current of battery can be expressed as:

$$i_{Lr}(t) = -V_{clamp}(t_6)\sqrt{\frac{C_1 + C_2}{L_r}}\sin\omega(t-t_6) \tag{18}$$

$$V_{clamp}(t) = V_{clamp}(t_6)\sqrt{\frac{L_r}{C_1 + C_2}}\cos\omega(t-t_6) \tag{19}$$

$$I_B = i_{La}(t_6) + i_{Lb}(t_6) \tag{20}$$

where $\omega = \sqrt{\frac{1}{L_r(C_1 + C_2)}}$. The equivalent circuit of mode 7 is shown in Figure 6g.

Mode 8 [Figure 6h, $t_7 < t < t_8$]:

At time t_7, the parasitic capacitor C_2 of the switch M_1 is charged to V_{clamp} and the parasitic capacitor C_1 of the switch M_1 is discharged down to zero. The inductor current i_{Lr} forces the body diode D_1 of M_1 conducting. When the body diode D_1 of the switch M_1 is conducted, a ZVS feature will be created for the switch M_1. The equivalent circuit of mode 8 is shown in Figure 6h.

At time t_8, the switch M_1 is turned on under ZVS condition. When the resonant inductor current i_{Lr} reaches zero, it will be forwarded and flow through the resonant inductor. Simultaneously, the battery is discharged again through the components (C_4, D_5, L_1, C_3 and M_3) of the non-dissipative reflex cell. The operation of the reflex charger over one switching cycle is completed.

3. Control Scheme Description

In order to achieve a fast dynamic response and high efficiency conversion, an optimal control scheme must be integrated into the proposed reflex charger. The optimal control scheme includes the maximum-power-point-tracking (MPPT) control algorithm of the PV panels and the ZVS control signals of the proposed reflex charger. In this section, the control scheme of the proposed reflex charger will be described in detail.

3.1. Description of the MPPT Algorithm

The PV cells are combined into PV panels. The equivalent circuit of a typical PV cell is shown in Figure 7. Since a PV cell produces less than 3 watts at approximately 0.5 V_{dc}, PV cell must be connected in series-parallel configurations to produce enough power for high-power applications. In the actual case, the I_{pv}-V_{pv} and P_{pv}-V_{pv} characteristic equations are expressed as follows:

$$I_{pv} = I_{ph} - I_D \tag{21}$$

or:

$$I_{pv} = n_p I_{ph} - n_p I_{sat}\left[\exp\left(\frac{q}{kTA}\frac{V_{pv}}{n_s}\right) - 1\right] \tag{22}$$

and:

$$P_{pv} = I_{pv}V_{pv} = n_p I_{ph}V_{pv} - n_p I_{sat}V_{pv}\left[\exp\left(\frac{q}{kTA}\frac{V_{pv}}{n_s}\right) - 1\right] \tag{23}$$

where n_p is the parallel number of the PV cells, n_s is the series number of the PV cells, I_{sat} is the reverse-saturation-current, I_{ph} is the output current of the PV panels, q is the electronic charge, k is Boltzmann's gas constant, T is the cell temperature of the PV panels and A is the ideality factor of the PV panels. From Equations (22) and (23), one can obtain I_{pv}-V_{pv} and P_{pv}-V_{pv} curves as shown in Figure 8.

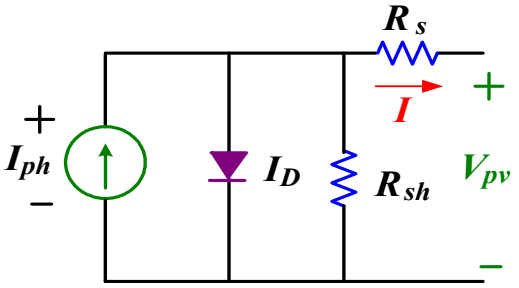

Figure 7. Equivalent circuit of PV cell.

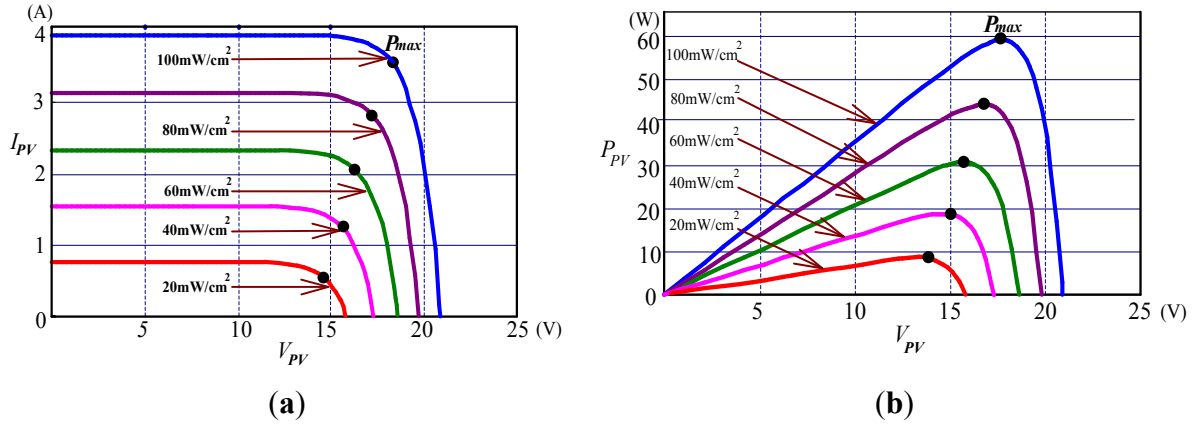

Figure 8. PV panels with different insolations: (**a**) I_{pv}-V_{pv} curves; and (**b**) P_{pv}-V_{pv} curves.

In Figure 8, it can be seen that the PV panels produce power only on illuminated isolation. There exists one operating point where the PV panels can generate their maximum output power P_{max}. From Figure 8, it can be seen that a common inherent drawback of the PV panels is the intermittent nature of their power. These drawbacks tend to make the PV panels inefficient. However, by incorporating MPPT algorithms, the power transfer efficiency of the PV panels can be improved significantly. In order to achieve the best energy utilization of the PV panels, MPPT algorithms and energy storage circuits must be integrated into battery charger. Figure 9 shows the conceptual diagram of the battery charger with an MPPT controller. The maximum power point P_{max} of PV panels can be obtained, as shown in Figure 10.

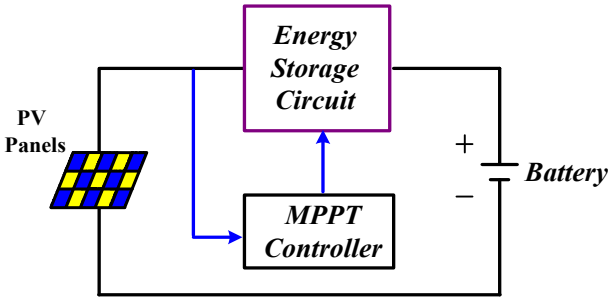

Figure 9. Conception diagram of battery charger for PV energy conversion.

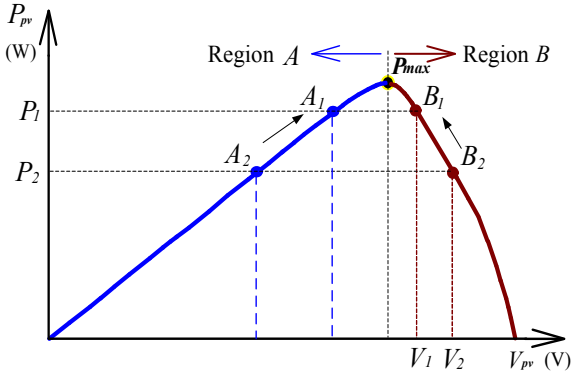

Figure 10. Maximum power point curve of PV panels with respect to V_{pv}.

In Figure 10, except for the maximum power point P_{max}, two possible operating regions A and B can be defined for a given P_{pv}. The current-operating-point location can be determined by a perturbation in the maximum power P_{max} of PV. Therefore, to achieve the best energy utilization of the PV panels, an MPPT algorithm with perturbation-and-observation method is usually adopted. The advantage of the perturbation-and-observation method is that MPPT controller only requires a few parameters to easily measure and control the maximum power point. Therefore, it is often applied to PV panels for enhancing the power capacity [5–9].

3.2. ZVS Cell Description

To reduce switching losses and increase conversion efficiency, a dc-dc converter with ZVS cells is usually adopted. The ZVS cell requires four main components, including an active switch, a passive diode, an inductor and a capacitor, as shown in Figure 11a. In general, an active switch is used to replace its passive diode, and then the ZVS cell can be modified as shown in Figure 11b. From Figure 11b,

a basic ZVS cell consists of two bidirectional active switches M_1 and M_2, two resonant capacitors C_1 and C_2, a resonant inductor L_r and a clamping capacitor C_{clamp}. The ZVS cell allows its inductor current i_{Lr} flowing in bidirectional manner, which can achieve ZVS features for active switches. Based on this ZVS feature, the topology of the proposed reflex charger with ZVS cell is composed, as shown in Figure 3. In Figure 3, to reduce the switching losses of the active switches (M_1 and M_2), the proposed reflex charger is necessary to store enough energy in the resonant inductor L_r to achieve ZVS at the turn-on transition of the switches. The ZVS condition of active switches can be obtained as the following inequality:

$$L_r \geq \frac{(C_1 // C_2)\ (V_{in})^2}{(i_{Lr})^2} \tag{24}$$

When the value of the parasitic capacitors is equal ($C_1 = C_2 = C$), the inequality can be expressed as follows:

$$L_r \geq \frac{2C\ (V_{in})^2}{(i_{Lr})^2} \tag{25}$$

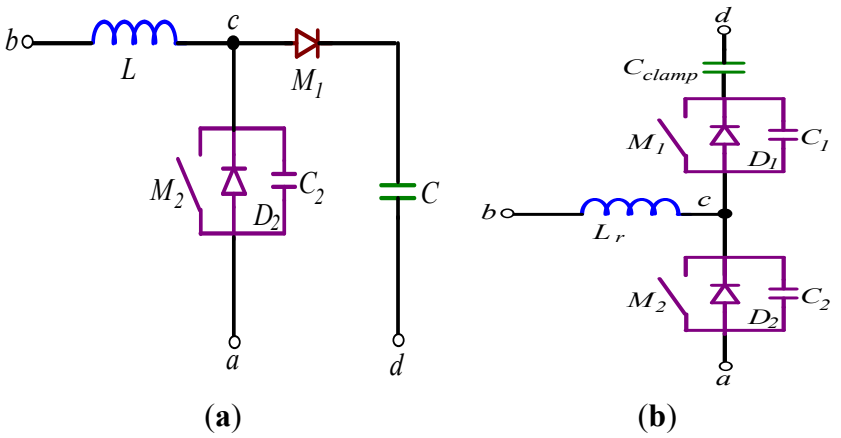

Figure 11. Illustration of a ZVS cell.

3.3. Description of a Non-Dissipative Charging/Discharging Reflex Cell

A non-dissipative charging/discharging reflex cell consists of passive switches, inductors and capacitors. Figure 12a shows the original concept of a bidirectional charging cell. In Figure 12a, the capacitors C_1 and C_2 are treated as energy buffers, the current tank I is treated as a charging current for the energy buffers, and the switches S_1 and S_2 are treated as charging switches of the energy buffers. In Figure 12a, the switches S_1 and S_2 can be identified as passive diode D_1 and D_2, and the current tank can be identified as an inductor L_1, as shown in Figure 12b. To obtain the charging/discharging function Figure 12b can be modified as shown in Figure 12c. In Figure 12c, to prevent from charging current following through inductor L_1, the extra passive diode D_3 is in series with the inductor L_1. Based on this illustration, the topology of the proposed charger with a non-dissipative charging/discharging reflex cell is composed, as shown in Figure 13.

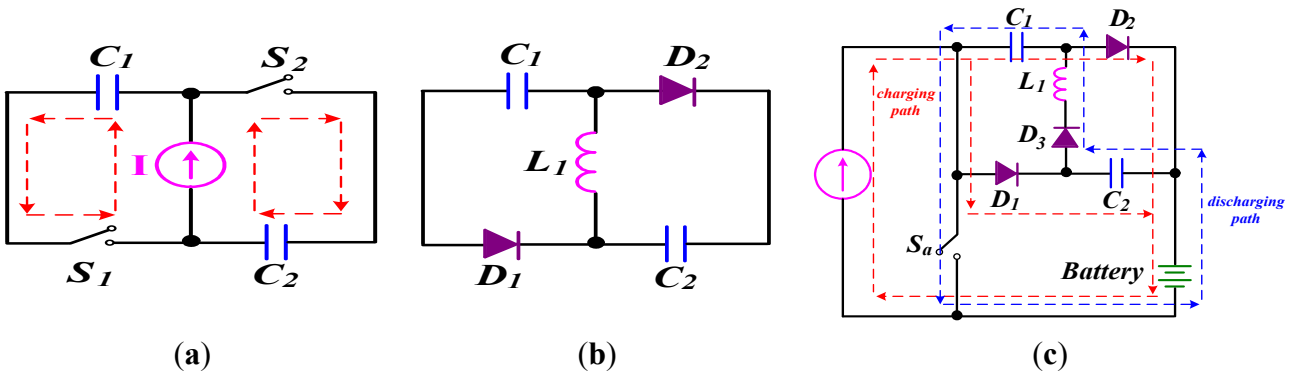

Figure 12. Illustration of a non-passive charging/discharging reflex cell: (**a**) original concept of bidirectional charging cell; (**b**) modified charging/discharging cell; (**c**) proposed charging/discharging reflex cell

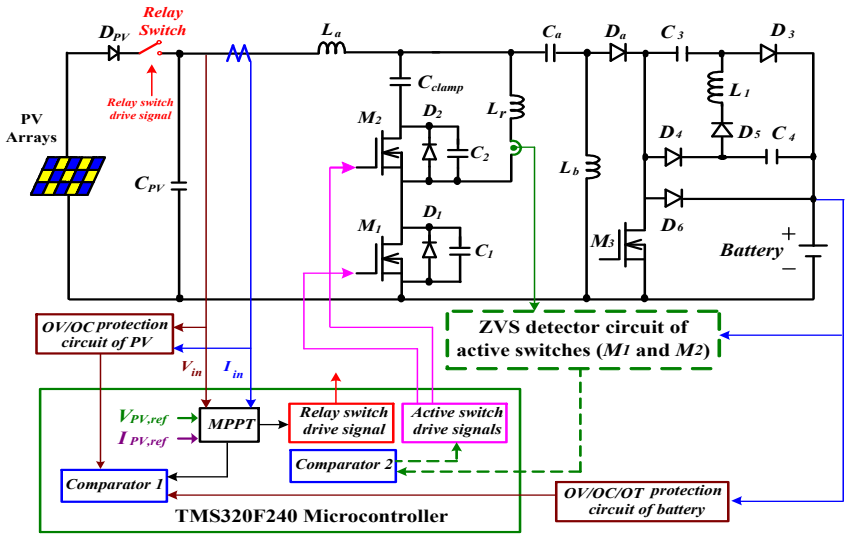

Figure 13. Conceptual control block diagram of the proposed reflex charger for PV energy conversion.

To achieve the optimal stability and safety of the proposed reflex charger, the functions of under-voltage, over-voltage, over-current, and over-temperature protection circuits are required. For cost considerations and best control, the MPPT algorithm and all the protection signals of the proposed reflex charger are implemented on the TMS320F240 microcontroller along with auxiliary analog circuits. The conceptual control block diagram of the proposed reflex charger for PV energy conversion is shown in Figure 13.

4. Experimental Results

In Figure 13, to verify the performance of the proposed reflex charger with ZVS and non-dissipative cells for the PV energy conversion, its specifications are listed as follows:

- Voltage of PV arrays: V_{pv} = 100 V_{dc};
- Voltage of Lead-Acid battery: V_B = 12 V_{dc}, capacity = 4 Ah;
- Maximum charging current of Lead-Acid battery: I_B = 2 A;
- Inductor L_a = L_b = 3 mH;

- Inductor L_1 = 5 μH;
- Resonant inductor L_r = 5 μH;
- Capacitor C_3 =C_4 = 300 *n*F; and
- Switching frequency (M_1 and M_2): f_s = 50 kHz.

Figure 14 shows measured output currents, voltages and their corresponding powers from start-up to the steady state for PV panels with the perturbation-and-observation MPPT method. In Figure 14, it can be observed that the maximum power point can be always obtained from PV panels. Figures 15 and 16 show the voltage and current waveforms of the main switch M_1 and auxiliary switch M_2. In Figures 15 and 16, it can be seen that the main switch M_1 and auxiliary switch M_2 have ZVS features during turn-on transition. Therefore, the switching losses of main switch M_1 and auxiliary switch M_2 can be eliminated during turn-on transition. Figure 17 shows measured charge/discharge current waveforms of battery under charging/discharging reflex cycle. Figure 18 shows measured charging voltage curve of battery, in which it can be seen that the battery can be improved by the proposed reflex charger in a short time.

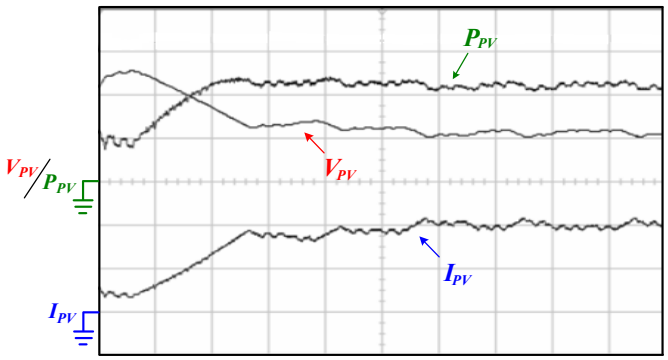

Figure 14. Measured output voltage, current and power waveforms of PV panels with perturbation-and-observation MPPT method. (V_{PV}: 100 V/div; P_{PV}: 50 W/div; I_{PV}: 0.5 A/div; time: 5 s/div).

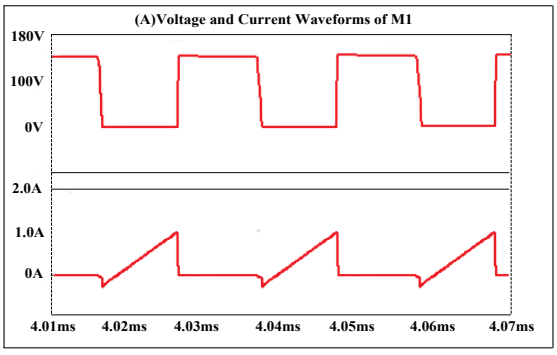

($V_{ds(M1)}$: 50 V/div; $i_{ds(M1)}$: 1 A/div; time: 10 μ s/div)

(**a**)

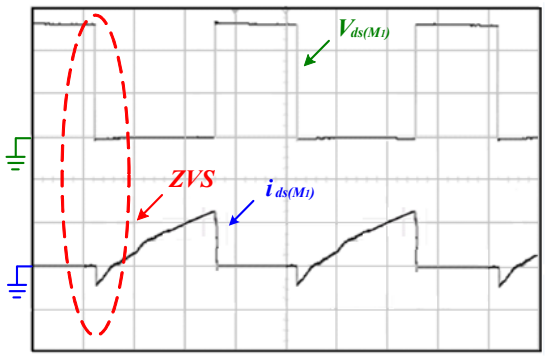

($V_{ds(M1)}$: 50 V/div; $i_{ds(M1)}$: 1 A/div; time: 10 μ s/div)

(**b**)

Figure 15. Voltage and current waveforms of main switch M_1: (**a**) simulated results; (**b**) experimental results.

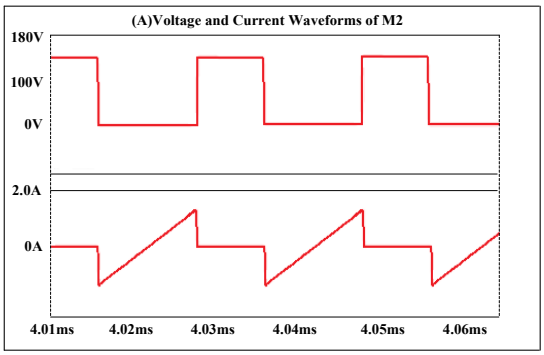

($V_{ds(M2)}$: 50 V/div; $i_{ds(M2)}$: 1 A/div; time: 10 μ s/div)

(**a**)

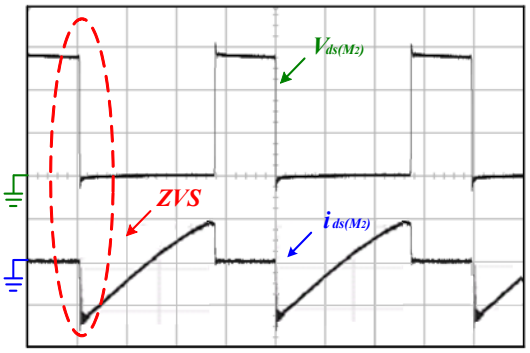

($V_{ds(M2)}$: 50 V/div; $i_{ds(M2)}$: 1 A/div; time: 10 μ s/div)

(**b**)

Figure 16. Voltage and current waveforms of main switch M_2: (**a**) simulated results; (**b**) experimental results.

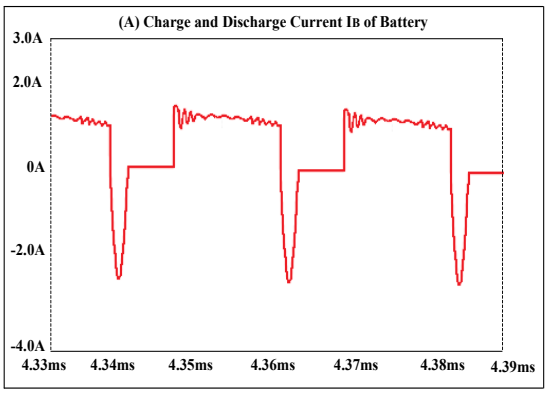

(I_B: 1 A/div; time: 10 μ s/div)

(**a**)

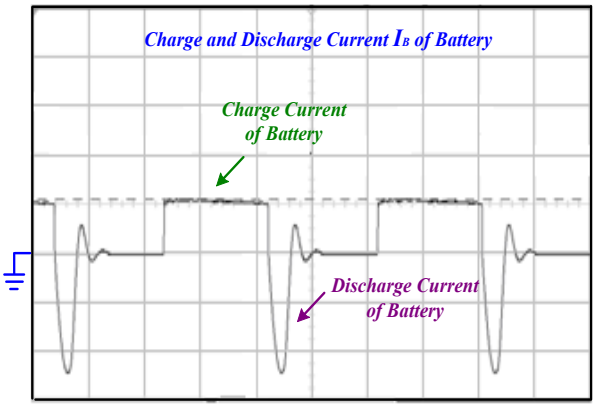

(I_B: 1 A/div; time: 10 μ s/div)

(**b**)

Figure 17. Charge and discharge current waveforms of battery: (**a**) simulated results; (**b**) experimental results.

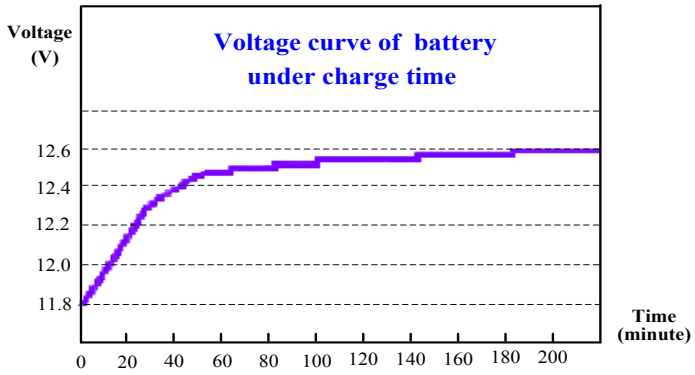

Figure 18. Measured voltage curve of battery under charge time.

Figure 19 shows efficiency measurements of the proposed reflex charger with ZVS and non-dissipative reflex cells, in which it can be seen that the maximum efficiency can be reached as high as 92% under ZVS condition.

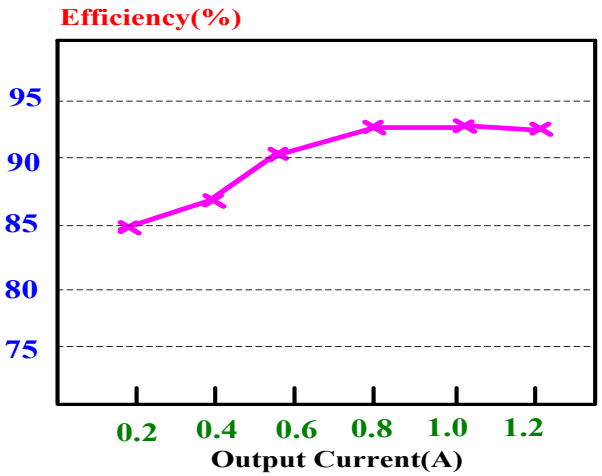

Figure 19. Efficiency of the proposed reflex charger with ZVS and non-dissipative cells.

5. Conclusions

In this paper, a reflex charger with ZVS and non-dissipative cells for PV energy conversion is proposed. The active switches of the proposed reflex charger have a ZVS feature at turn-on transition. Hence, the switching losses of the active switches can be ignored. The non-dissipative reflex cell uses only passive elements, which can increase charging efficiency and extend the battery lifecycle. In order to draw maximum power from PV arrays, a simple perturbation-and-observation method is incorporated to realize maximum power conversion. To achieve the optimal stability, safety and cost effective of the proposed reflex charger, the protected circuits and MPPT algorithms consist of a microcontroller (TMS320F240, Texas Instruments, Dallas, TX, USA) to implement maximum power conversion and protect the battery charger. Experimental results have been verified that the proposed reflex charger with ZVS and non-dissipative cells is relatively suitable for PV energy conversion.

Acknowledgments

This work was supported by the National Science Council, Taiwan, under Grant No. MOST 103-2221-E-167-031.

Author Contributions

All of the authors contributed to publishing this paper. Cheng-Tao Tsai wrote the paper and Ying-Che Kuo, Ying-Piao Kuo and Chin-Tsung Hsieh contributed to part of the writing and editing work of the manuscript.

Conflicts of Interest

The authors declare no conflict of interest.

References

1. Bull, S.R. Renewable energy today and tomorrow. *Proc. IEEE* **2001**, *89*, 1216–1226.

2. World Wind Energy Association. *World Wind Energy Report 2008*; World Wind Energy Association: Bonn, Germany, 2009.
3. Ahmed, K.H.; Finney, S.J.; Williams, B.W. Fuzzy-logic-control approach of a modified hill-climbing method for maximum power point in microgrid standalone photovoltaic system. *IEEE Trans. Power Electron.* **2011**, *26*, 1022–1030.
4. Tseng, S.-U.; Tsai, C.-T. Photovoltaic power system with an interleaving boost converter for battery charger applications. *Int. J. Photoenergy* **2012**, *2012*, 1–15.
5. Chao, K.H.; Chang, L.Y.; Liu, H.C. Maximum-power-point-tracking method based on modified particle swarm optimization for photovoltaic systems. *Int. J. Photoenergy* **2013**, *2013*, 1–6.
6. Tang, K.H.; Chao, K.H.; Chao, Y.W.; Chen, J.P. Design and implementation of a simulator for photovoltaic modules. *Int. J. Photoenergy* **2012**, *2012*, 1–8.
7. Kuo, Y.-C.; Liang, T.-J.; Chen, J.-F. Novel maximum-power-point-tracking controller for photovoltaic energy conversion system. *IEEE Trans. Ind. Electron.* **2001**, *48*, 594–601.
8. Koyanagi, A.; Nakamura, H.; Kobayashi, M.; Suzuki, Y. Study on maximum power point tracking of wind turbine generator using a flywheel. *Proc. Power Convers.* **2002**, *1*, 322–327.
9. Amei, K.; Takayasu, Y.; Ohji, T.; Sakui, M. A maximum power control of wind generator system using a permanent magnet synchronous generator and a boost chopper circuit. *Proc. Power Convers.* **2002**, *3*, 1447–1452.
10. Shen, C.-L.; Tsai, C.-T. Double-linear approximation algorithm to achieve maximum-power-point tracking for photovoltaic arrays. *Energies* **2012**, *5*, 1982–1997.
11. Teleke, S.; Baran, M.E.; Huang, A.Q.; Bhattacharya, S.; Anderson, L. Control strategies for battery energy storage for wind farm dispatching. *IEEE Trans. Energy Convers.* **2009**, *24*, 725–731.
12. Cao, J.; Schofield, N.; Emadi, A. Battery balancing methods: A comprehensive review. In Proceedings of the IEEE Vehicle Power and Propulsion Conference, Harbin, China, 3–5 September 2008.
13. Chiu, H.-J.; Lin, L.-W.; Pan, P.-L.; Tseng, M.-H. A novel rapid charger for lead-acid batteries with energy recovery. *IEEE Trans. Power Electron.* **2006**, *21*, 640–647.
14. Hsieh, Y.C.; Moo, C.S.; Wu, C.K.; Cheng, J.C. A non-dissipative reflex charging circuit. In Proceeding of the 25th International Telecommunications Energy Conference, INTELEC ’03, Yokohama, Japan, 23–23 October 2003; pp. 679–683.
15. Chen, L.-R.; Chu, N.-Y.; Wang, C.-S.; Liang, R.-H. Design of a reflex-based bidirectional converter with the energy recovery function. *IEEE Trans. Ind. Electron.* **2008**, *55*, 3022–3029.
16. Zhang, J.; Yu, J.; Cha, C.; Yang, H. The effects of pulse charging on inner pressure and cycling characteristics of sealed Ni/MH batteries. *J. Power Sources* **2004**, *136*, 180–185.
17. Yabuta, K.; Matsushita, T.; Tsujikawa, T. Examination of the cycle life of valve regulated lead acid batteries. In Proceedings of the 29th International Telecommunications Energy Conference, INTELEC 2007, Rome, Italy, 30 September–4 October 2007; pp. 97–101.
18. Tsai, C.-T. Energy storage system with voltage equalization strategy for wind energy conversion. *Energies* **2012**, *5*, 2331–2350.
19. Patel, H.; Agarwal, V. MPPT scheme for a PV-fed single-phase single-stage grid-connected inverter operating in CCM with only one current sensor. *IEEE Trans. Energy Convers.* **2009**, *24*, 256–263.

20. Moore, S.W.; Schneider, P.J. A review of cell equalization methods for lithium ion and lithium polymer battery system. In Proceedings of the SAE 2001 World Congress, Detroit, MI, USA, 12 March 2001.
21. Lee, Y.S.; Chen, G.T. ZCS bi-directional DC-to-DC converter application in battery equalization for electric vehicles. In Proceedings of the IEEE Power Electronics Specialists Conference, Rhodes, Greece, 15–19 June 2004; Volume 4, pp. 2766–2772.
22. Lee, Y.S.; Chen, M.-W.; Hsu, K.-L.; Du, J.-Y.; Chuang, C.-F. Cell equalization scheme with energy transferring capacitance for series connected battery strings. In Proceedings of the IEEE TenCon'02, 2002 IEEE Region 10 Conference on Computers, Communications, Control and Power Engineering, Beijing, China, 28–31 October 2002; pp. 2042–2045.
23. Cho, J.G.; Baek, J.W.; Yoo, D.W.; Lee, H.S.; Rim, G.H. Novel zero-voltage and zero-current-switching full bridge PWM converter using transformer auxiliary winding. *IEEE Trans. Power Electron.* **2000**, *15*, 250–257.
24. Lo, Y.K.; Kao, T.S.; Lin, J.K. Analysis and design of an interleaved active-clamp forward converter. *IEEE Trans. Ind. Electron.* **2007**, *54*, 2323–2332.